Convolutional Neural Network-Based Prediction of Reflection Response for Free-Form Antenna Designs

Bartosz Czaplewski [0000-0001-7904-5567]

Department of Teleinformation Networks, Faculty of Electronics, Telecommunications and Informatics, Gdansk University of Technology, Narutowicza 11/12, 80-233 Gdansk, Poland
bartosz.czaplewski@pg.edu.pl

Abstract. This work introduces a convolutional neural network capable of estimating the reflection response of 50-vertex free-form planar antennas across the 3–8 GHz band. By directly inferring electromagnetic behavior from geometry, the proposed approach eliminates reliance on expert-driven design rules and electromagnetic simulations. This is the first study employing machine learning to predict the complete frequency-dependent reflection response of complex free-form antenna structures. The contributions include: (i) a publicly available dataset comprising 108,710 pseudo-random antenna geometries and their corresponding reflection responses; (ii) a convolutional neural network that maps complex antenna shapes to wideband reflection characteristics; and (iii) an experimental analysis covering performance metrics and comparison with alternatives. Antenna geometries are encoded as a 2×51 tensor of vertex coordinates, while the network outputs 251 reflection coefficient values sampled at 20 MHz intervals over the 3–8 GHz range. Model hyperparameters were determined using Bayesian optimization, and robustness was assessed through 10-fold cross-validation and evaluation on an independent test set. The proposed model attains a mean squared error of 3.789 $(\text{dB})^2$, a mean absolute error of 0.902 dB, and a coefficient of determination of 0.437 over the considered frequency band. With an average inference time of 6.06 ms, the framework supports rapid screening of large design populations, effectively removing electromagnetic simulation as a bottleneck during early-stage exploration.

Keywords: Machine Learning, Convolutional Neural Networks, Reflection Response Regression, Antenna Design Evaluation.

1 Introduction

Wireless communication systems rely on antennas as interfaces that determine system performance under constraints such as miniaturization and multiband operation. Traditionally, antenna design relies on iterative, experience-driven procedures involving geometry selection and parametric tuning, typically supported by electromagnetic (EM) simulations. These approaches are time-consuming and influenced by engineering bias, which favors reusing familiar topologies and heuristics, thereby limiting exploration of unconventional yet potentially effective designs. Engineering bias,

ICCS Camera Ready Version 2026
To cite this paper please use the final published version:
DOI: 10.1007/978-3-032-29921-5_12

understood as reliance on intuition accumulated through experience [1, 2], arises because topology development is largely a cognitive task: engineers form an implicit sense of viable solutions and preferentially select known shapes. This restricts early-stage exploration, where maintaining configuration diversity could enable discovery of high-performance but uncommon topologies.

One approach to mitigating engineering bias is the automatic generation of antenna topologies directly from design specifications, without direct human intervention. Existing approaches either refine predefined topologies [3, 4] or generate structures under general constraints [5, 6]. Although the latter strategy increases design flexibility, it typically requires extensive EM simulations, thereby motivating the development of tools for early-stage topology selection. This paper proposes a method that supports the automation of the design process of freeform antenna topologies through a data-driven regression model that predicts the reflection response over a wide frequency range, without relying on canonical forms or expert assumptions.

Free-form antenna geometries are represented either as compositions of primitive shapes [7–11] or as sets of coordinate points [12–15]. Matrix-based representations use binary grids to activate or deactivate elements, ensuring connectivity through overlap, while point-based approaches define the radiator via interconnected vertices. Both representations require high-dimensional parameter spaces to achieve flexibility. High dimensionality incurs significant computational cost. Consequently, simulation-driven optimization becomes impractical due to the need for thousands of EM evaluations [12, 14, 16, 17]. Surrogate-assisted optimization can alleviate this burden [12, 18], but its effectiveness depends on suitable initial designs, leaving the problem of bias-free identification of viable starting points unresolved [19–23].

Machine learning (ML) enables data-driven modeling and optimization across telecommunications [24–30]. In antenna design, ML can accelerate development, reduce computational cost, and approximate EM behavior [28, 31, 32]. However, most existing methods focus on optimizing predefined structures, offering limited support for early-stage exploration. This motivates the need for ML tools that identify promising free-form antenna topologies from scratch, without assumptions or costly simulations.

The goal of this work is to build a model predicting the reflection response of high-dimensional pseudo-random free-form antenna designs without expert bias or EM simulations. The objective is to estimate the reflection coefficient rapidly and accurately, replacing time-consuming EM simulations. The proposed approach employs a convolutional neural network (CNN) that takes an antenna geometry and directly predicts the return loss ($20 \cdot \log_{10}|S_{11}(f)|$) over 3–8 GHz with 20 MHz resolution. Rather than predicting performance at a single frequency, the model predicts reflection across the band, enabling rapid screening of thousands of antennas per minute.

The contributions are: (1) a new dataset of 108,710 pseudo-random free-form antenna topologies paired with EM-simulated reflection responses; (2) a CNN predicting reflection magnitude over 3–8 GHz from 50-vertex geometries; and (3) a thorough experimental evaluation including training, hyperparameter tuning, and performance analysis. To the authors' knowledge, this is the first AI model predicting wideband reflection response for high-dimensional free-form antennas without parametric simplifications, expert-driven features, or reliance on canonical designs.

ICCS Camera Ready Version 2026
To cite this paper please use the final published version:
DOI: 10.1007/978-3-032-29921-5_12

2 Related Work

In [10], a CNN regression model was proposed to predict the two resonant frequencies of a dual-band pixelated microstrip antenna. The antenna geometry was represented by an 8×6 binary matrix encoding the presence or absence of metallization, allowing for non-conventional shapes while reducing engineering bias. Unfortunately, the full reflection response was not considered. The model outputs a 1×2 vector of resonant frequencies and was trained on 1,940 dual-band antennas, limiting generalization beyond structures with exactly two resonances. The reported mean relative errors were 0.13% for the first resonant frequency and 0.22% for the second.

In [33], a CNN was proposed for rapid prediction of antenna EM responses using a pole–residue transfer function. The study considered a conventional ultra-wideband (UWB) monopole with a band notch, described by four geometric parameters. Binary cross-sectional images (415×214) serve as input, while the network outputs TF coefficients enabling reconstruction of $|S_{11}(f)|$ over 2–12 GHz. The dataset was limited (64 training, 49 test samples), no quantitative error metrics were reported, and performance was assessed only through visual comparison with EM simulations.

In [34], a progressive Gaussian process was used to model monopole antennas, reducing the need for costly EM simulations by iteratively adding high-variance samples to the training set. The model's outputs were $|S_{11}|$ or voltage standing wave ratio at a single frequency. Two simple antennas were studied: a 3-parameter L-shaped slot and a 4-parameter UWB inverted-U slot. Full frequency responses require pointwise evaluation. Average metrics reported were: MAE = 0.431, r = 0.993 for L-shaped; MAE = 0.289, r = 0.958 for inverted-U. Datasets were limited (13 and 30 samples).

In [35], a CNN combined with particle swarm optimization (PSO) was proposed for designing complex antennas and predicting resonant frequencies. The input was a 12×12 binary matrix representing the metallization layout, capturing sufficiently complex, non-conventional geometries to reduce engineering bias. The output consisted of reflection response samples. The model was trained on 500 antenna topologies with corresponding S11 simulations. No quantitative metrics were reported; performance was evaluated via visual comparison of predicted and simulated S_{11} plots.

In [36], early-stage antenna evaluation was framed as a multi-label classification problem rather than direct regression of reflection responses. A multi-layer perceptron (MLP) took free-form, pseudo-random antennas with 50 vertices as input. The output was a 10-bit binary vector indicating whether the antenna is a promising candidate (reflection < –3 dB over ≥10% bandwidth) in each 0.5 GHz sub-band from 3–8 GHz. Moreover, a dataset comprising 106,351 samples was introduced, and the model achieved 93.55% accuracy in both label-specific and overall evaluations.

In [37], a CNN was proposed to predict antenna operational frequency ranges from 256×256 binary maps of pseudo-random 50-vertex designs as a multi-label classification problem. Alongside a dataset of 136,351 designs labeled over ten 0.5 GHz bands from 3 to 8 GHz, a CNN architecture featuring six convolutional and four fully connected layers was proposed for processing high-dimensional binary inputs. The model achieved a macro-averaged test accuracy of 0.9387.

ICCS Camera Ready Version 2026
To cite this paper please use the final published version:
DOI: 10.1007/978-3-032-29921-5_12

Comparing the two methods above with the approach proposed here, in [36, 37] the task is multi-label classification of antenna operability in specific sub-bands, whereas in the present work the task is regression, predicting the full frequency-dependent reflection response. Furthermore, [36, 37] use different datasets, and the representation of antenna topologies differs significantly.

In [38], a CNN was used to model resonant frequencies of rectangular microstrip antennas (RMSA) from 4×10 binary images encoding four geometric parameters, rather than using physical 2D representations. The output was limited to the resonant frequency, and the simple rectangular geometry and tiny dataset (33 samples) constrained generalization. Reported performance included an average percentage error of 0.482%, RMSE of 54.43 MHz, and R^2 of 0.9977, though the CNN's spatial modeling potential was underutilized, as no spatial patterns were present in the input.

3 Methodology

The proposed approach maps a parametric antenna description to its frequency-dependent reflection response using a CNN. The proposed approach maps a parametric antenna description to its frequency-dependent reflection response using a CNN. Each antenna geometry is encoded into a numerical representation that serves as the network input, while the output corresponds to the predicted reflection response over the 3–8 GHz frequency range. Network input and output are detailed in Section 5.

To determine an optimal network configuration, Bayesian optimization (BO) was first applied. This stage was carried out using the Optuna framework with a tree-structured Parzen Estimator strategy. The optimization explored a constrained but expressive search space, including the number of convolutional layers (2–5), the number of channels in the convolutional layers (8–8192) with controlled growth in subsequent layers. Kernel sizes in the initial convolutional layer were selected from odd values between 3 and 15, with optional reductions in deeper layers. The fully connected part of the network was defined by 1–4 layers, starting with 512–4096 neurons and allowing systematic reductions in later layers. Additional hyperparameters included the activation function (ReLU, Leaky ReLU, or ELU), dropout rate (0.0–0.2), learning rate, and weight decay. Logical constraints were imposed to exclude implausible architectures while maintaining sufficient diversity in the search space. Each candidate configuration was trained on 70% of the dataset and evaluated on a validation subset comprising 20% of the data. Early stopping and learning rate scheduling were employed to improve optimization efficiency. The hyperparameter set (see Section 5) yielding the lowest validation loss was selected and carried forward to the next stage. The BO procedure was conducted over 500 trials.

The selected architecture was assessed using 10-fold cross-validation on 90% of the dataset. This provided a more reliable estimate of expected performance by reducing sensitivity to a single data split and ensuring that all samples contributed to training and validation. Mean squared error was monitored during each fold, and average metrics were computed across folds. No additional retraining on the full dataset was performed, and the best-performing fold-specific model was directly used for testing.

ICCS Camera Ready Version 2026
To cite this paper please use the final published version:
DOI: 10.1007/978-3-032-29921-5_12

The final performance assessment (see Section 6) was conducted on a strictly held-out test set containing the remaining 10% of the dataset, which was entirely disjoint from both the BO and cross-validation stages. Model performance was quantified using mean squared error (MSE), mean absolute error (MAE), coefficient of determination (R^2), and root mean squared error (RMSE) evaluated over the 3–8 GHz frequency range and at selected frequency points with 0.5 GHz spacing.

4 Dataset

This study presents a newly constructed large-scale dataset comprising 108,710 entries, where each record pairs a quasi-random, high-complexity free-form antenna geometry with its numerically simulated reflection response. The dataset is publicly available in [39], and representative samples are shown in Figure 1.

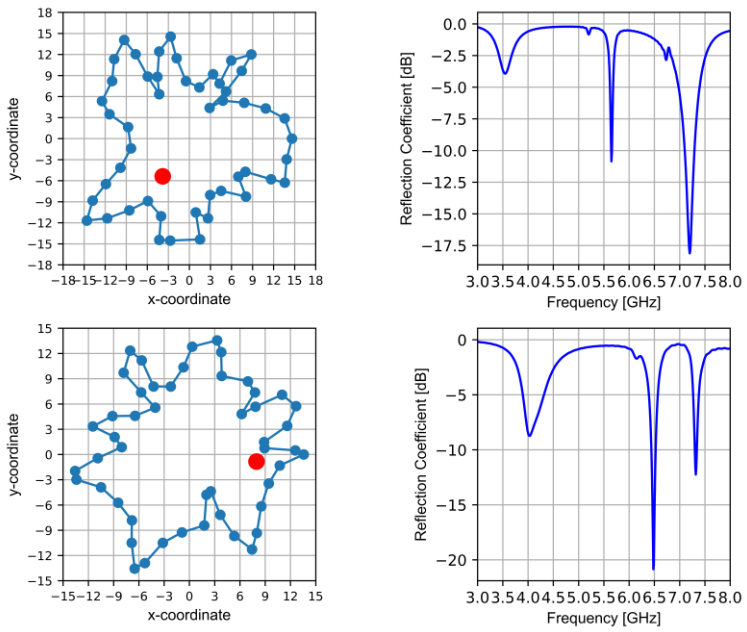

Fig. 1. Examples of antenna designs and corresponding reflection responses in the dataset.

Antenna topologies were generated under constraints ensuring EM simulation feasibility, specifically: continuous metallic geometries without internal voids; randomized radial distances and angular increments within predefined bounds; smooth, polar-convex, non-self-intersecting shapes; and a feed point location randomly selected within the antenna boundary. The feed point is the location where the transmission line is connected, providing the electrical excitation to the radiating structure.

ICCS Camera Ready Version 2026
To cite this paper please use the final published version:
DOI: 10.1007/978-3-032-29921-5_12

Each antenna design is encoded as a 102-element vector D = [q_x, v_x, q_y, v_y], where (q_x, q_y) denote the Cartesian coordinates of the feed point, while $\mathbf{v}_x$ = [$v_{x,1}$,…,$v_{x,50}$] and $\mathbf{v}_y$ = [$v_{y,1}$,…,$v_{y,50}$] represent the x- and y-coordinates of the 50 contour vertices in the xy-plane. All coordinates range from −20 to +20 mm.

The reflection characteristics were computed via full-wave electromagnetic simulations spanning the 3–8 GHz frequency band. The simulations were performed in CST Microwave Studio [40] using a finite integration technique–based solver [7–9]. Each reflection response is a 251-element vector of $S_{11}(f)$ samples, expressed in decibels as $20\cdot\log_{10}|S_{11}(f)|$, at 20 MHz intervals across the 3–8 GHz frequency range.

5 Model

The ordered coordinate representation motivates the use of a 1-dimensional CNN to capture local spatial dependencies across input channels. The input is a 2×51 tensor describing the antenna geometry, with one channel containing the x-coordinates and the other the y-coordinates. The first coordinate pair specifies the feed location, while the remaining pairs define the 50 vertices. The network outputs 251 samples of the reflection response, $20\cdot\log_{10}(|S_{11}(f)|)$, over the 3–8 GHz frequency range with a 20 MHz resolution. Inputs are z-score standardized per coordinate channel, while the outputs are standardized per frequency. The model's architecture is given in Table 1.

Table 1. Structure hyperparameters

Layer type	Hyperparameters	Output
Input	-	2 × 51
Conv1D	512 channels, kernel 5, stride 1, padding 2, leaky ReLU	512 × 51
Max Pooling	kernel 2	512 × 25
Conv1D	512 channels, kernel 3, stride 1, padding 1, leaky ReLU	512 × 25
Max Pooling	kernel 2	512 × 12
Conv1D	1024 channels, kernel 3, stride 1, padding 1, leaky ReLU	1024 × 12
Max Pooling	kernel 2	1024 × 6
Conv1D	4096 channels, kernel 3, stride 1, padding 1, leaky ReLU	4096 × 6
Max Pooling	kernel 2	4096 × 3
Conv1D	4096 channels, kernel 3, stride 1, padding 1, leaky ReLU	4096 × 3
Max Pooling	kernel 2	4096 × 1
Flatten	-	1 × 4096
Fully Connected	1024 neurons, leaky ReLU	1 × 1024
Fully Connected	512 neurons, leaky ReLU	1 × 512
Fully Connected	512 neurons, leaky ReLU	1 × 512
Fully Connected	512 neurons, leaky ReLU	1 × 512
Output (FC)	251 neurons, no activation function	1 × 251

ICCS Camera Ready Version 2026
To cite this paper please use the final published version:
DOI: 10.1007/978-3-032-29921-5_12

The proposed network comprises 70,663,419 trainable parameters and is organized into two functional stages: feature extraction stage using one-dimensional convolutional layers, and prediction stage based on fully connected layers. Architectural choices, including the number of convolutional layers, channel widths, kernel sizes, depth and width of the fully connected part, as well as the selected activation functions, were determined through BO (see Section 3). Max-pooling operations were incorporated to reduce feature dimensionality, improve computational efficiency, and promote better generalization.

The network was trained using the Adam optimizer. L2 regularization was incorporated to limit overfitting, promote more robust feature representations, and enhance generalization. Dropout layers were also evaluated during BO but were found to be detrimental and were therefore omitted from the final architecture, as the model was already effectively regularized through L2 and its size was optimized. A learning rate scheduler was applied to stabilize convergence and prevent overshooting during training. Early stopping was also used to curtail overfitting and reduce training duration. Learning hyperparameters are listed in Table 2.

Table 2. Learning hyperparameters

Learning parameter	Value
Batch size	64
Solving algorithm	Adam
Initial learning rate	5e−4
Weight decay (L2 regularization)	1e−4
Learning rate (LR) scheduler	ReduceLROnPlateau (mode='min')
LR scheduler factor	0.1
LR scheduler patience	5
Loss function	Mean Square Error
Max epochs	1000
Early stopping validation patience	10

6 Results

Figure 2 presents the reflection responses obtained from EM simulations (blue), which serve as the reference, together with the predicted responses (red) produced by the model. The results demonstrate the model's capacity to rapidly generate reflection responses that closely approximate the simulation outputs, allowing for swift estimation of an antenna's operational frequency range from its pseudo-random free-form geometry. Visual comparison indicates a high overall fidelity between predictions and simulated curves. However, minor discrepancies exist: narrow low-reflection bands at higher frequencies are occasionally missed, and closely spaced narrow bands can sometimes appear as a single broader band. Despite these limitations, the prediction accuracy is sufficient to support preliminary design evaluation.

ICCS Camera Ready Version 2026
To cite this paper please use the final published version:
DOI: 10.1007/978-3-032-29921-5_12

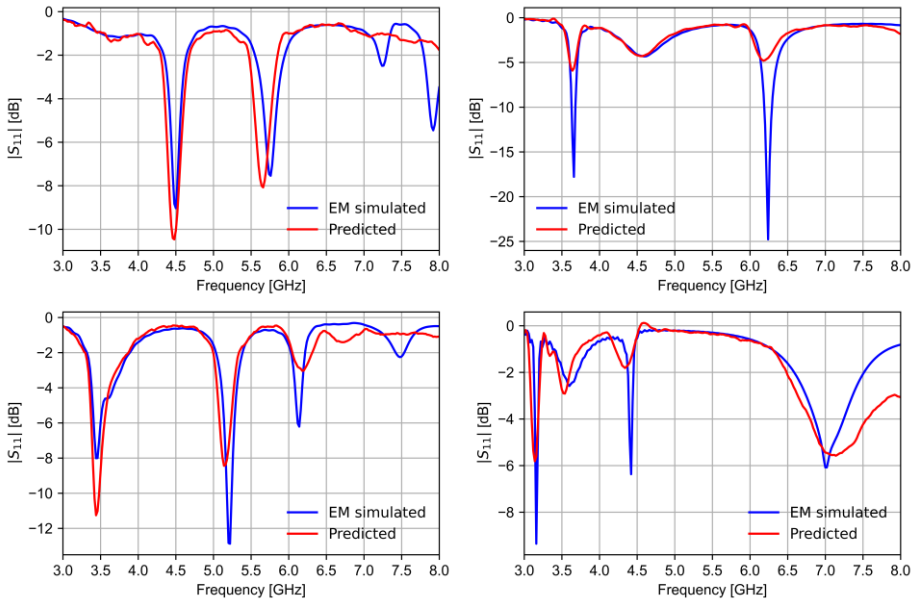

Fig. 2. Examples of reflection response prediction.

Table 3 summarizes the test results, reporting MSE, MAE, R^2, and RMSE averaged over all frequency points across the full 3–8GHz range. These metrics reflect the model's overall performance in predicting the complete frequency-dependent responses. The proposed method achieved an MSE of 3.789 $(dB)^2$, an MAE of 0.902 dB, an R^2 of 0.437, and an RMSE of 1.947 dB.

Table 4 reports the test results evaluated at discrete frequency points from 3 GHz to 8 GHz in 0.5 GHz increments. The model demonstrates high predictive accuracy for frequencies up to 6.0 GHz, with MAE remaining below 0.62 dB and RMSE below 1.43 dB. The best performance is observed at 4.5 GHz, where MSE = 1.201 $(dB)^2$, MAE = 0.455 dB, R^2 = 0.721, and RMSE = 1.096 dB. At higher frequencies, from 6.5 GHz onward, the metrics gradually deteriorate, reaching their lowest values at 8.0 GHz, where MSE = 10.831 $(dB)^2$, MAE = 2.174 dB, R^2 = 0.202, RMSE = 3.291 dB, which reflects the increased resonance complexity in this frequency range.

Table 5 shows that the average processing time per sample is approximately 6 ms. CPU preprocessing includes loading the antenna design, converting it to a PyTorch tensor, applying per-channel standardization, and transferring the data to the GPU. GPU inference corresponds to a single model evaluation with gradients disabled. CPU postprocessing involves transferring outputs back to the CPU, detaching gradients, and performing per-frequency de-standardization. Total time spans from initial data retrieval from RAM to completion of prediction.

All training, validation, and testing procedures were implemented in Python 3.11 using PyTorch 2.5.1 with CUDA 11.8 support and executed on NVIDIA GeForce RTX 3080 GPU. However, time measurements were performed on a workstation equipped with an Intel i7-4790K CPU and an NVIDIA GeForce GTX 1080 Ti GPU.

ICCS Camera Ready Version 2026
To cite this paper please use the final published version:
DOI: 10.1007/978-3-032-29921-5_12

Table 3. Evaluation results over the full frequency range

Testing Metric	Value
MSE	3.789 $(dB)^2$
MAE	0.902 dB
R^2	0.437
RMSE	1.947 dB

Table 4. Evaluation results at selected frequencies

Frequency	MSE $[(dB)^2]$	MAE [dB]	R^2	RMSE [dB]
3.0 GHz	0.613	0.215	0.496	0.783
3.5 GHz	1.932	0.617	0.649	1.390
4.0 GHz	1.847	0.604	0.721	1.359
4.5 GHz	1.201	0.455	0.721	1.096
5.0 GHz	1.454	0.478	0.628	1.206
5.5 GHz	1.734	0.510	0.545	1.317
6.0 GHz	2.028	0.596	0.436	1.424
6.5 GHz	4.554	1.051	0.386	2.134
7.0 GHz	7.237	1.558	0.350	2.690
7.5 GHz	9.987	1.953	0.258	3.160
8.0 GHz	10.831	2.174	0.202	3.291

Table 5. Mean processing time per sample

Processing Stage	Proposed CNN	EM simulation
CPU preprocessing	0.225 ms	N/A
GPU processing	2.382 ms	N/A
CPU postprocessing	3.449 ms	N/A
Total time	6.063 ms	~60-90 s

7 Comparison

A straightforward comparison with existing studies is not feasible, as the present work is, to the author's knowledge, the first to address prediction of the complete reflection response across a broad frequency band for pseudo-random free-form antenna geometries. Earlier contributions have largely concentrated on reduced problem formulations, such as estimating resonant frequencies or reflection coefficients at discrete frequency points, and have typically been limited to canonical antenna shapes of low geometrical complexity. To establish a comparison that is both fair and informative, only methods satisfying a set of strict criteria were considered: the use of a similar design space based on pseudo-random two-dimensional free-form layouts, operation

ICCS Camera Ready Version 2026
To cite this paper please use the final published version:
DOI: 10.1007/978-3-032-29921-5_12

over a compatible frequency range, and the availability of sufficient implementation details to enable retraining on the dataset introduced in this study. Under these constraints, three regression-based approaches reported in [10, 33, 38] and three classification-based methods from [36, 37] were selected for quantitative assessment.

To establish a regression-based reference, three previously reported regression models [10, 33, 38] were implemented and appropriately adapted. In particular, adjustments to the input and output dimensionalities were introduced to ensure compatibility with the dataset described in Section 4. Following these modifications, each model was retrained to perform the regression task of estimating the reflection response associated with free-form antenna geometries defined by 50 vertices.

The quantitative comparison with regression methods is summarized in Table 6. The proposed CNN demonstrates superior performance relative to previously published models, achieving consistently lower error values across all considered metrics, including MSE, MAE, and RMSE, while simultaneously yielding a markedly higher coefficient of determination (R^2). The regression approaches reported in [10, 33, 38] were initially developed as computationally efficient predictors for canonical or geometrically simple antennas and therefore do not possess sufficient representational capacity to model the high-dimensional and irregular design space investigated in this study. This outcome highlights an inherent limitation of earlier regression frameworks: their reliance on simplified geometries and compact architectures tends to perpetuate engineering bias and restricts their applicability when exploring non-standard antenna configurations. Although effective for conventional patch- or dipole-type structures, such methods do not scale to the diverse and highly complex geometries considered here. Consequently, the results confirm that the proposed CNN is not only quantitatively superior but also well suited for facilitating unbiased exploration of antenna designs in previously underexplored regions of the design space.

Table 6. Comparison against regression methods

Metric	Proposed CNN	Retrained [10]	Retrained [38]	Retrained [33]
Learnable parameters	70,663,419	67,391	215,661	123,057
MSE	3.789 $(dB)^2$	6.074 $(dB)^2$	5.734 $(dB)^2$	5.529 $(dB)^2$
MAE	0.902 dB	1.416 dB	1.331 dB	1.302 dB
R^2	0.437	0.098	0.149	0.179
RMSE	1.947 dB	2.465 dB	2.395 dB	2.351 dB

Within the scope of classification methods, three neural network architectures, referred to here as MLP#1 [36], MLP#2 [36], and a 2D-CNN [37], were trained using large datasets of randomly generated antenna geometries to address a multi-label classification task. The input representations consist of pseudo-random free-form antenna designs defined by 50 vertices, encoded as a 103-element vector for MLP#1 and MLP#2, and as a binary 256 × 256 matrix for the 2D-CNN. The networks produce 10-bit output label vectors, with each bit associated with a 0.5 GHz frequency sub-band

ICCS Camera Ready Version 2026
To cite this paper please use the final published version:
DOI: 10.1007/978-3-032-29921-5_12

covering the range from 3.0 GHz to 8.0 GHz. Each label indicates whether a given antenna design constitutes a promising candidate for further optimization within the corresponding sub-band. As defined in [36, 37], a promising candidate exhibits a reflection coefficient below −3 dB over a relative bandwidth of at least 10%.

To ensure a fair and meaningful comparison with the aforementioned multi-label classification approaches, the output of the proposed CNN, i.e. the frequency-wide predicted reflection response, was analyzed to derive a binary 10-bit label vector that is equivalent to the label representation employed by the multi-label classification methods in [36, 37]. Based on the resulting label vectors, several performance metrics were evaluated, including accuracy, precision, recall, specificity, and the F1 score. All of these metrics were computed using macro-averaging, i.e., as the mean of per-label values. In addition, the exact-match accuracy was reported, which requires the predicted 10-bit label vector to be identical to the corresponding ground-truth vector.

A comparison with the classification approaches is presented in Table 7. Values reported in parentheses correspond to 95% confidence intervals (CI), which were estimated using non-parametric bootstrap resampling over the test set. The results indicate that the proposed CNN attains the highest macro-average accuracy (0.957) as well as the highest exact-match accuracy (0.654). This performance reflects its superior capability to capture the overall frequency-dependent characteristics of antenna responses and to correctly identify all relevant sub-bands.

It should be emphasized that this classification-oriented evaluation does not constitute the primary objective of the proposed CNN. The principal contribution of the model is its ability to predict the complete reflection coefficient response over a densely sampled frequency range, thereby offering a substantially richer and more flexible characterization of antenna behavior than that provided by purely classification methods. Nonetheless, the strong performance observed in the classification comparison underscores the robustness and versatility of the proposed approach.

Table 7. Comparison against classification methods

Metric (95% CI)	Proposed CNN	MLP#1 [36]	MLP#2 [36]	2D-CNN [37]
Learnable parameters	70,663,419	129,327,626	29,814,794	48,751,050
Accuracy	0.957 (0.956–0.958)	0.935 (0.933–0.937)	0.933 (0.931–0.935)	0.939 (0.937–0.940)
Precision	0.528 (0.507–0.549)	0.768 (0.761–0.775)	0.765 (0.758–0.772)	0.718 (0.710–0.725)
Recall	0.637 (0.615–0.659)	0.756 (0.749–0.762)	0.738 (0.730–0.745)	0.698 (0.691–0.706
Specificity	0.967 (0.966–0.968)	0.964 (0.963–0.965)	0.965 (0.964–0.966)	0.968 (0.967–0.969)
F1 score	0.571 (0.553–0.589)	0.761 (0.754–0.767)	0.749 (0.743–0.756)	0.702 (0.695–0.708)
Exact-match accuracy	0.654 (0.645–0.662)	0.629 (0.620–0.638)	0.602 (0.593–0.611)	0.605 (0.596–0.613)

ICCS Camera Ready Version 2026
To cite this paper please use the final published version:
DOI: 10.1007/978-3-032-29921-5_12

8 Conclusions

The proposed model is a practical and computationally efficient component of a modern antenna design workflow. It can serve both as a fast surrogate evaluator in local or global optimization loops and as a filtering mechanism for geometry generators conditioned on target operating bands. In either role, the model enables informed decision-making at stages where rapid feedback is critical.

A key advantage of the approach lies in its ability to replace costly EM simulations during the early exploration phase. Across the full frequency span, the model achieves an MSE of 3.789 $(\text{dB})^2$, an MAE of 0.902 dB, an RMSE of 1.947 dB, and an R^2 score of 0.437, with performance in the mid-band approaching levels suitable for preliminary screening. Crucially, inference requires, on average, 6 ms per antenna topology—compared to approximately 60–90 seconds for a single EM simulation—thereby enabling the evaluation of thousands of candidate geometries per minute and eliminating the main computational bottleneck in shape-space exploration. Although the overall R^2 is moderate, the model achieves high accuracy up to 6 GHz, which defines its reliable operating range, while final designs still require EM validation.

Unlike pointwise regression or binary feasibility classification in prior works, the proposed model predicts the entire reflection coefficient response. Specifically, it outputs the $20 \cdot \log_{10}|S_{11}(f)|$ curve sampled at 251 frequency points between 3 GHz and 8 GHz with a 20 MHz resolution. This representation allows direct assessment of key antenna characteristics, including impedance bandwidth, resonance depth, and passband continuity, thereby providing a substantially richer and more actionable signal for design decisions than scalar or categorical outputs.

Finally, the adopted data generation strategy reduces engineering bias at the concept formation stage. Training on a new dataset comprising 108,710 pseudo-random polygonal geometries with 50 vertices and randomly positioned feed points exposes the model to rarely explored shapes. By covering unconventional regions of the design space, the model facilitates the discovery of non-intuitive antenna topologies and supports a broader, less constrained search for high-performance solutions.

The overarching objective is to develop an integrated, multi-stage ML framework for fully automated antenna synthesis that eliminates the need for engineering expertise and computationally expensive EM simulations. Within this framework, the first stage [36, 37], focused on rapid preliminary assessment by predicting the operational frequency range of free-form antenna designs. The present work constitutes the second stage. In the short term, future work related to this stage will investigate alternative shape representations and encoding strategies. In the longer term, the framework will be extended with the third and fourth stages. The third stage will introduce a generative model capable of synthesizing antenna geometries conditioned on target frequency bands, with performance evaluation provided by models from the first and second stages. The fourth stage will incorporate an optimization model responsible for the iterative refinement of the antenna topologies generated in the third stage.

Disclosure of Interests. The author has no competing interests to declare that are relevant to the content of this article.

ICCS Camera Ready Version 2026
To cite this paper please use the final published version:
DOI: 10.1007/978-3-032-29921-5_12

References

1. Bandler, J.: Space Mapping-Have You Ever Wondered About the Engineer's Mysterious "Feel" for a Problem? [Speaker's Corner]. IEEE Microwave. 19, 112–122 (2018). https://doi.org/10.1109/MMM.2017.2780722.
2. Mroczka, J.: The cognitive process in metrology. Measurement. 46, 2896–2907 (2013). https://doi.org/10.1016/j.measurement.2013.04.040.
3. Ghassemi, M., Bakr, M., Sangary, N.: Antenna design exploiting adjoint sensitivity-based geometry evolution. IET Microwaves Antenna & Prop. 7, 268–276 (2013). https://doi.org/10.1049/iet-map.2012.0374.
4. Bekasiewicz, A., Kurgan, P., Koziel, S.: Numerically Efficient Miniaturization-Oriented Optimization of an Ultra-Wideband Spline-Parameterized Antenna. IEEE Access. 10, 21608–21618 (2022). https://doi.org/10.1109/ACCESS.2022.3152736.
5. Bekasiewicz, A., Dzwonkowski, M., Dhaene, T., Couckuyt, I.: Specification-Oriented Automatic Design of Topologically Agnostic Antenna Structure. In: Franco, L., De Mulatier, C., Paszynski, M., Krzhizhanovskaya, V.V., Dongarra, J.J., and Sloot, P.M.A. (eds.) Computational Science – ICCS 2024. pp. 11–18. Springer Nature Switzerland, Cham (2024). https://doi.org/10.1007/978-3-031-63759-9_2.
6. Bekasiewicz, A., Askaripour, K.: Performance Comparison of Automatically Generated Topologically Agnostic Patch Antennas. In: 2024 25th International Microwave and Radar Conference (MIKON). pp. 143–146. IEEE, Wroclaw, Poland (2024). https://doi.org/10.23919/MIKON60251.2024.10633953.
7. Ding, M., Jin, R., Geng, J., Wu, Q., Yang, G.: Auto-design of band-notched UWB antennas using mixed model of 2D GA and FDTD. Electron. Lett. 44, 257–258 (2008). https://doi.org/10.1049/el:20082056.
8. Trinh-Van, S., Yang, Y., Lee, K.-Y., Hwang, K.: A Wideband Circularly Polarized Pixelated Dielectric Resonator Antenna. Sensors. 16, 1349 (2016). https://doi.org/10.3390/s16091349.
9. Li, C., Xu, S., Yang, F., Li, M.: Design and Optimization of a Mechanically Reconfigurable Reflectarray Antenna with Pixel Patch Elements Using Genetic Algorithm. In: 2019 IEEE MTT-S International Wireless Symposium (IWS). pp. 1–3. IEEE, Guangzhou, China (2019). https://doi.org/10.1109/IEEE-IWS.2019.8804092.
10. Jacobs, J.P.: Accurate Modeling by Convolutional Neural-Network Regression of Resonant Frequencies of Dual-Band Pixelated Microstrip Antenna. Antennas Wirel. Propag. Lett. 20, 2417–2421 (2021). https://doi.org/10.1109/LAWP.2021.3113389.
11. Wu, G.-B., Zeng, Y.-S., Chan, K.F., Chen, B.-J., Qu, S.-W., Chan, C.H.: High-Gain Filtering Reflectarray Antenna for Millimeter-Wave Applications. IEEE Trans. Antennas Propagat. 68, 805–812 (2020). https://doi.org/10.1109/TAP.2019.2943432.
12. Bekasiewicz, A., Koziel, S., Plotka, P., Zwolski, K.: EM-Driven Multi-Objective Optimization of a Generic Monopole Antenna by Means of a Nested Trust-Region Algorithm. Applied Sciences. 11, 3958 (2021). https://doi.org/10.3390/app11093958.
13. Whiting, E.B., Campbell, S.D., Mackertich-Sengerdy, G., Werner, D.H.: Dielectric Resonator Antenna Geometry-Dependent Performance Tradeoffs. IEEE Open J. Antennas Propag. 2, 14–21 (2021). https://doi.org/10.1109/OJAP.2020.3037826.

ICCS Camera Ready Version 2026
To cite this paper please use the final published version:
DOI: 10.1007/978-3-032-29921-5_12

14. Lizzi, L., Viani, F., Azaro, R., Massa, A.: Optimization of a Spline-Shaped UWB Antenna by PSO. Antennas Wirel. Propag. Lett. 6, 182–185 (2007). https://doi.org/10.1109/LAWP.2007.894157.
15. Alroughani, H., McNamara, D.A.: The Shape Synthesis of Dielectric Resonator Antennas. IEEE Trans. Antennas Propagat. 68, 5766–5777 (2020). https://doi.org/10.1109/TAP.2020.2988984.
16. Alnas, J., Giddings, G., Jeong, N.: Bandwidth Improvement of an Inverted-F Antenna Using Dynamic Hybrid Binary Particle Swarm Optimization. Applied Sciences. 11, 2559 (2021). https://doi.org/10.3390/app11062559.
17. Koziel, S., Bekasiewicz, A.: Comprehensive Comparison of Compact UWB Antenna Performance by Means of Multiobjective Optimization. IEEE Trans. Antennas Propagat. 65, 3427–3436 (2017). https://doi.org/10.1109/TAP.2017.2700044.
18. Koziel, S., Bekasiewicz, A.: Multi-Objective Design of Antennas Using Surrogate Models. WORLD SCIENTIFIC (EUROPE) (2017). https://doi.org/10.1142/q0043.
19. Koziel, S., Ogurtsov, S.: Multi-Objective Design of Antennas Using Variable-Fidelity Simulations and Surrogate Models. IEEE Trans. Antennas Propagat. 61, 5931–5939 (2013). https://doi.org/10.1109/TAP.2013.2283599.
20. Koziel, S., Bekasiewicz, A.: Fast multi-objective design optimization of microwave and antenna structures using data-driven surrogates and domain segmentation. EC. 37, 753–788 (2019). https://doi.org/10.1108/EC-01-2019-0004.
21. Koziel, S., Bekasiewicz, A.: Domain segmentation for low-cost surrogate-assisted multi-objective design optimisation of antennas. IET Microwaves Antenna & Prop. 12, 1728–1735 (2018). https://doi.org/10.1049/iet-map.2017.0635.
22. Koziel, S., Bekasiewicz, A.: Rapid Simulation-Driven Multiobjective Design Optimization of Decomposable Compact Microwave Passives. IEEE Trans. Microwave Theory Techn. 64, 2454–2461 (2016). https://doi.org/10.1109/TMTT.2016.2583427.
23. Koziel, S., Bekasiewicz, A.: Multi-objective optimization of expensive electromagnetic simulation models. Applied Soft Computing. 47, 332–342 (2016). https://doi.org/10.1016/j.asoc.2016.05.033.
24. Yang, H., Zeng, R., Xu, G., Zhang, L.: A network security situation assessment method based on adversarial deep learning. Applied Soft Computing. 102, 107096 (2021). https://doi.org/10.1016/j.asoc.2021.107096.
25. Shen, S., Cai, C., Li, Z., Shen, Y., Wu, G., Yu, S.: Deep Q-network-based heuristic intrusion detection against edge-based SIoT zero-day attacks. Applied Soft Computing. 150, 111080 (2024). https://doi.org/10.1016/j.asoc.2023.111080.
26. Mohammadian, H., Ghorbani, A.A., Lashkari, A.H.: A gradient-based approach for adversarial attack on deep learning-based network intrusion detection systems. Applied Soft Computing. 137, 110173 (2023). https://doi.org/10.1016/j.asoc.2023.110173.
27. Huang, J., Nan, J., Gao, M., Wang, Y.: Antenna modeling based on meta-heuristic intelligent algorithms and neural networks. Applied Soft Computing. 159, 111623 (2024). https://doi.org/10.1016/j.asoc.2024.111623.
28. Shang, Y., Deng, W., Liu, J., Ma, J., Shang, Y., Dai, J.: Long term 5G base station traffic prediction method based on spatial-temporal correlations. Applied Soft Computing. 167, 112333 (2024). https://doi.org/10.1016/j.asoc.2024.112333.

ICCS Camera Ready Version 2026
To cite this paper please use the final published version:
DOI: 10.1007/978-3-032-29921-5_12

29. Baz, A., Logeshwaran, J., Natarajan, Y., Patel, S.K.: Enhancing mobility management in 5G networks using deep residual LSTM model. Applied Soft Computing. 165, 112103 (2024). https://doi.org/10.1016/j.asoc.2024.112103.
30. Panek, M., Pomykała, A., Jabłoński, I., Woźniak, M.: 5G/5G+ network management employing AI-based continuous deployment. Applied Soft Computing. 134, 109984 (2023). https://doi.org/10.1016/j.asoc.2023.109984.
31. Khan, M.M., Hossain, S., Mozumdar, P., Akter, S., Ashique, R.H.: A review on machine learning and deep learning for various antenna design applications. Heliyon. 8, e09317 (2022). https://doi.org/10.1016/j.heliyon.2022.e09317.
32. Sarker, N., Podder, P., Mondal, M.R.H., Shafin, S.S., Kamruzzaman, J.: Applications of Machine Learning and Deep Learning in Antenna Design, Optimization, and Selection: A Review. IEEE Access. 11, 103890–103915 (2023). https://doi.org/10.1109/ACCESS.2023.3317371.
33. Luo, H.-Y., Hong, Y., Lv, Y.-H., Shao, W.: Parametric Modeling of UWB Antennas Using Convolutional Neural Networks. In: 2020 IEEE International Symposium on Antennas and Propagation and North American Radio Science Meeting. pp. 2055–2056. IEEE, Montreal, QC, Canada (2020). https://doi.org/10.1109/IEEECONF35879.2020.9329697.
34. Zheng, X., Meng, F., Tian, Y., Zhang, X.: Design of monopole antennas based on progressive Gaussian process. Int. J. Microw. Wireless Technol. 15, 255–262 (2023). https://doi.org/10.1017/S1759078722000125.
35. Zhang, X., Tian, Y., Zheng, X.: Optimal Design of Fragment-Type Antenna Structure Based on PSO-CNN. In: 2019 International Applied Computational Electromagnetics Society Symposium - China (ACES). pp. 1–2. IEEE, Nanjing, China (2019). https://doi.org/10.23919/ACES48530.2019.9060460.
36. Czaplewski, B.: Neural Network for Evaluating the Operational Range of Antennas with Randomly Generated Designs. In: Lees, M.H., Cai, W., Cheong, S.A., Su, Y., Abramson, D., Dongarra, J.J., and Sloot, P.M.A. (eds.) Computational Science – ICCS 2025. pp. 394–402. Springer Nature Switzerland, Cham (2025). https://doi.org/10.1007/978-3-031-97635-3_47.
37. Czaplewski, B.: A convolutional neural network for predicting the frequency range of antennas based on randomized designs. Engineering Applications of Artificial Intelligence. 165, 113561 (2026). https://doi.org/10.1016/j.engappai.2025.113561.
38. Fu, H., Tian, Y., Meng, F., Li, Q., Ren, X.: Microstrip antenna modelling based on image-based convolutional neural network. Electronics Letters. 59, e12910 (2023). https://doi.org/10.1049/ell2.12910.
39. Czaplewski, B.: 1Ddesign-to-response-2.8 - Free-Form Antenna Designs with Reflection Responses, https://zenodo.org/doi/10.5281/zenodo.16784875, (2025). https://doi.org/10.5281/ZENODO.16784875.
40. CST Microwave Studio, (2019).

ICCS Camera Ready Version 2026
To cite this paper please use the final published version:
DOI: 10.1007/978-3-032-29921-5_12